IOP Publishing | International Atomic Energy Agency Nuclear Fusion

Nucl. Fusion **62** (2022) 076006 (14pp) https://doi.org/10.1088/1741-4326/ac62f6

To dee or not to dee: costs and benefits of altering the triangularity of a steady-state DEMO-like reactor

J.A. Schwartz[1,*], **A.O. Nelson**[2] and **E. Kolemen**[1,*]

[1] Princeton University, Department of Mechanical and Aerospace Engineering, United States of America
[2] Columbia University, Department of Applied Physics and Applied Mathematics, United States of America

E-mail: jacobas@princeton.edu and ekolemen@princeton.edu

Received 15 October 2021, revised 1 March 2022
Accepted for publication 31 March 2022
Published 9 May 2022

Abstract

Shaping a tokamak plasma to have a negative triangularity may allow operation in an edge-localized mode-free L-mode regime and with a larger strike-point radius, ameliorating divertor power-handling requirements. However, the shaping has a potential drawback in the form of a lower no-wall ideal beta limit, found using the MHD codes CHEASE and DCON. Using the new fusion systems code FAROES, we construct a steady-state DEMO2 reactor model. This model is essentially zero-dimensional and neglects variations in physical mechanisms like turbulence, confinement, and radiative power limits, which could have a substantial impact on the conclusions deduced herein. Keeping its shape otherwise constant, we alter the triangularity and compute the effects on the levelized cost of energy (LCOE). If the tokamak is limited to a fixed B field, then unless other means to increase performance (such as reduced turbulence, improved current drive efficiency or higher density operation) can be leveraged, a negative-triangularity reactor is strongly disfavored in the model due to lower β_N limits at negative triangularity, which leads to tripling of the LCOE. However, if the reactor is constrained by divertor heat fluxes and not by magnet engineering, then a negative-triangularity reactor with higher B_0 could be favorable: we find a class of solutions at negative triangularity with lower peak heat flux and lower LCOE than those of the equivalent positive triangularity reactors.

Keywords: triangularity, cost, economics, fusion reactor, magnetohydrodynamics, tokamak

(Some figures may appear in colour only in the online journal)

1. Introduction

Shape is critical for determining tokamak plasma behavior. The effects of aspect ratio A and elongation κ have both been extensively studied [1–4] and their impacts on reactors [5, 6] understood. After A and κ, the third most common quantity used to describe the shape of a tokamak plasma is the triangularity, often denoted as δ. A plasma with $\delta = 0$ has a vertical symmetry when viewed in the poloidal plane, while one with positive δ is flatter on the inboard side and more rounded on the outboard side, like the letter D, and a plasma with $\delta < 0$ is shaped like a backward D. Modern large tokamaks, including JET, NSTX-U, and DIII-D, have been constructed to primarily support positive triangularity shapes, and increased positive triangularity has been found to yield improved performance [7], including access to higher energy confinement times via H-mode [8–10].

However, designing a reactor to run in H-mode is challenging due to the onset of edge-localized modes (ELMs) in this high performance regime [11–13]. If not mitigated [14, 15], these releases of energy can damage divertor components with extreme transient heat fluxes [16]. In an encouraging development, recent experiments have demonstrated

* Authors to whom any correspondence should be addressed.

ELM-free negative-triangularity L-mode plasmas with confinement times comparable to those of positive-triangularity H-mode plasmas [17, 18]. Avoiding ELMs permits a steadier and more manageable heat flux at the divertor, and the geometry of negative triangularity permits an increased strike point radius, further lowing heat fluxes. Remaining in L-mode also avoids the necessity of maintaining a power through the separatrix high enough to prevent an H $\rightarrow$ L mode back-transition; this power must then be radiated in the SOL or handled in the divertor.

These attributes have led to a renewed interest [19] in negative-triangularity reactors [20, 21], which were recently reviewed by Marinoni *et al* [22]. The potential of a negative triangularity reactor is further increased by recent advancements in magnet technology permitting higher fields [23, 24], which may compensate for lower $\langle\beta_N\rangle$ achievable with negative triangularity. It would be useful to have some metric by which to compare positive and negative triangularity reactors.

This paper examines the economic consequences of moving from positive to negative triangularity for a DEMO-like reactor. In particular, we focus on the levelized cost of energy (LCOE). This is the constant price such that if a plant is operated at its maximum power, P_{net}, over the fraction of the year it is available, f_{av}, and sells all the produced electricity at this price, the lifetime costs of constructing and operating the plant will be exactly recouped. It can be computed as

$$\mathrm{LCOE} = \frac{C_{C0}F_{CR0} + C_{OM}}{8760 f_{av} P_{net}} + C_V, \tag{1}$$

where C_{C0} is the total capital cost of the plant, F_{CR0} is the annualized fixed charge rate to pay for the capital, C_{OM} is the annual fixed operations and maintenance cost, and C_V is the variable cost of operation per MW h. As an optimization objective, LCOE can be preferable to capital cost, since it takes into account these operational costs and lower availability due to scheduled maintenance.

A novel fusion systems code, FAROES, is used to construct a zero-dimensional tokamak model including several effects of triangularity. The model does *not* include variation of plasma profiles, such as an H-mode with a pedestal at positive triangularity and an L-mode without pedestal without triangularity, nor does it include variation in core confinement or radiative fraction limits, which are potentially favorable for negative triangularity, nor consider how plasma physics mechanisms like energetic particle confinement or current drive efficiency change with shape. Additionally, since the model is zero-dimensional, the points presented here do not necessarily correspond to a real-world combination of self-consistent plasma profiles, which must be produced and controlled via the actuators available in a power plant. Additional experiments and more sophisticated simulations must be performed to establish and evaluate reactor-grade negative triangularity plasmas.

A cost model [25] incorporated into FAROES calculates the capital cost, operational costs, and availability of the reactor, leading to the calculation of the LCOE. However, we report here only the relative costs of different design points. The cost model is heavily simplified, and does not account for expected future developments necessary for the deployment of fusion at scale. While it has value for comparing similar designs under the same set of assumptions, the true cost of fusion energy will depend on many factors including technological progress which is underway.

We find that the best choice of triangularity depends on the relative capabilities of magnet technology and divertor technology. For example, at constant toroidal field B_{T0}, the decreased fusion power due to the lower β_N limit at negative triangularity nearly triples the LCOE, which cannot be mitigated by a lower plant downtime due to lower peak divertor heat loads. However, we also find that if the toroidal field can be *increased* without incurring significant additional capital costs, there are negative triangularity solutions with equal fusion power but lower peak divertor heat loads *and* a lower LCOE.

To begin this investigation, we review some strengths and weaknesses of negative triangularity reactors in section 2. The new systems code FAROES is then introduced in section 3 along with a discussion of the effects of triangularity which are implemented in the tokamak model used for the present study. Section 4 presents the results of altering the DEMO-like reactor from positive to negative triangularity with a fixed B_{T0}, and section 5 studies the effects of changing B_{T0}. In these studies, we see that configurations with positive or negative triangularity can both emerge as the favored geometry depending on the most relevant technological drivers, as summarized in section 6. Finally, initial conclusions from this study are presented in section 7.

2. Strengths and weakness of negative triangularity

The attributes of negative triangularity reactors which are key to this study are described in this section. For a more detailed introduction see Kikuchi [26] and Marinoni *et al* [22].

Tokamaks with negative triangularity are potentially useful because they can achieve high confinement while operating in an ELM-free L-mode regime [17, 19, 20], which alleviates issues with extreme transient heat fluxes and plasma–material interactions, simplifying the divertor problem. With the divertor x-point at a larger radius, divertor power-handling is further eased as the plasma-wetted area is larger. For fixed profiles of temperature and density, the geometry of negative-triangularity flux surfaces is expected to lead to an enhanced bootstrap current [20], which decreases external current-drive requirements and can lead to a lower recirculating power fraction, especially for steady-state devices. Additionally, turbulent diffusion of heat due to trapped electron modes may be suppressed, leading to higher confinement factors H [27–29].

However, the geometry also has certain disadvantages compared with a positive-triangularity plasma. For example, more of the plasma exists at a large major radius, where the toroidal field is lower by $1/R$. This means that the averaged pressure achievable for a given $\langle\beta_T\rangle$ (volume-averaged beta) decreases, potentially leading to lowered plasma performance. Additionally, we find that the ideal no-wall stability limit is lower in $\langle\beta_N\rangle$ (normalized volume-averaged beta) for negative

triangularity, further decreasing plasma performance. This is in agreement with previous work by Medvedev *et al* on TCV, which showed that $n > 0$ modes in negative triangularity have a lower limit due to reduced wall stabilization [21, 30, 31]. Moving the tallest point of the confined plasma to a larger R may worsen the toroidal field ripple, leading to greater fast-particle losses through stochastic ripple banana-drift diffusion [32], unless the TF magnet bore size is increased as well. Moving more of the plasma to a larger R also increases the first wall area and blanket volume, and may lead to a less compact machine core, potentially increasing the capital costs associated with reactor designs.

3. Comparison methodology

We recreate the steady-state DEMO2 reactor described by Reux *et al* [33] using the new systems code FAROES. We then use Sheffield's updated tokamak plant cost model [25] to assess changes to the capital cost and LCOE, relative to the reference case. In section 4, we vary the triangularity while keeping fixed the rest of the radial build, plasma elongation, and toroidal field strength. Since the magnitudes of some physics effects of triangularity are not yet well-quantified (such as enhancements to H_{98}), or are only crudely estimated within our model (enhancements to trapped particle fractions and bootstrap current), we perform various scans, adjusting the magnitudes of some of these effects or keeping certain outputs constant, and let the code solve for self-consistent design points. In section 5 we study the effects of increasing the toroidal field strength.

3.1. Overview of the FAROES systems code

FAROES is a systems code for fusion reactors written in `python`, largely ported from spreadsheet models developed by Menard *et al* [6]. It is built using the multidisciplinary optimization framework OpenMDAO [34]. The FAROES tokamak model used in this work is zero-dimensional; i.e. quantities such as the total fusion rate are computed as a fixed constant times the plasma volume and the volume-averaged ion temperatures and densities. Inclusion of the Sheffield and Milora [25] cost model allows optimization for values such as the capital cost and LCOE. A manuscript describing FAROES is in preparation, and the effects of triangularity included in the tokamak model for this work are described in this section.

3.2. Effects of triangularity in the FAROES tokamak model

The FAROES tokamak model used for this study includes two types of effects of triangularity: purely-geometric effects and physics effects. Purely-geometric effects will be discussed first. The shape of the last closed flux surface (LCFS) is given by [35, 36]

$$R = R_0 + a\,\cos(t + \delta\,\sin\,t), \tag{2}$$

$$Z = \kappa a\,\sin(t), \tag{3}$$

where t ranges from 0 to 2π. This is a smooth shape without an X-point; while the model includes notional divertors, they are neglected in the geometric representation of the LCFS. It should also be noted that the major radius, R_0, is both the geometric axis (the mean of the inboard and outboard plasma radii) and the plasma axis; this model does not recognize a Shafranov shift. Here the quantity δ is referred to as the triangularity. Basic geometric effects with this plasma shape include a larger plasma volume and surface area at $\delta < 0$, as well as altered poloidal circumference and cross-sectional area. In this FAROES tokamak model, the first wall conforms to the plasma shape, so the blanket area and (at constant thickness) blanket volume are larger at negative δ as well, leading to increased material costs.

One geometric consequence of the negative triangularity shape is that more of the plasma is located at a larger major radius R, where the toroidal magnetic field is lower. It follows that for a given 'volume-averaged toroidal beta', $\langle\beta_\mathrm{T}\rangle$, the volume-averaged plasma pressure $\langle p\rangle_V$ will be lower for a negative triangularity shape. These quantities are defined and the effect described in more detail in the subsequent section.

3.2.1. Geometric effects on volume-averaged plasma pressure at fixed $\langle\beta_\mathrm{T}\rangle$ or fixed $\langle\beta_{\mathrm{N},v}\rangle$ and plasma current.

The standard ('experimentalist' [37]) toroidal beta is defined as

$$\beta_\mathrm{T} = \frac{\langle p\rangle_V}{B_{\mathrm{T0}}^2/2\mu_0}, \tag{4}$$

where $\langle p\rangle_V$ is the volume-averaged pressure within the LCFS and $B_{\mathrm{T0}}^2/2\mu_0$ is the pressure of the vacuum field at the geometric center of the plasma. This can also be thought of as the ratio of the total thermal energy of the plasma to the magnetic energy that would be in a plasma-sized volume with a uniform field of strength B_{T0},

$$\beta_\mathrm{T} = \frac{\int p\,\mathrm{d}V}{VB_{\mathrm{T0}}^2/2\mu_0}.$$

Troyon and Gruber [37] noted that there is a related 'numerically derived' variant to this quantity, which we call[3] $\langle\beta\rangle$. With B denoting the *local* field strength, it is

$$\langle\beta\rangle = \frac{\int p\,\mathrm{d}V}{\int B^2\,\mathrm{d}V/2\mu_0} = \frac{\langle p\rangle_V}{\langle B^2\rangle_V/2\mu_0}, \tag{5}$$

the ratio of the total thermal energy to the total (poloidal and toroidal field) magnetic energy within the LCFS. In the FAROES tokamak model, we use a third variant, denoted $\langle\beta_\mathrm{T}\rangle$,

$$\langle\beta_\mathrm{T}\rangle = \frac{\int p\,\mathrm{d}V}{\int B_{\mathrm{T},v}^2\,\mathrm{d}V/2\mu_0} = \frac{\langle p\rangle_V}{\langle B_{\mathrm{T},v}^2\rangle_V/2\mu_0}, \tag{6}$$

where $B_{\mathrm{T},v}$ is the local vacuum toroidal field. Its denominator is easier to compute because it does not involve the poloidal field or the perturbations to the toroidal field by the plasma, and for the plasmas considered here, $\langle\beta_\mathrm{T}\rangle$ is about 1% larger than $\langle\beta\rangle$. Compared to β_T, $\langle\beta_\mathrm{T}\rangle$ decenters B_{T0}, which is useful because we might expect that physical results like MHD stability limits are more naturally expressed in terms of ratios of

[3] Note that $\langle\cdot\rangle$ used without the subscript $_V$ is not a true volume average, but is a ratio of volume-averaged quantities.

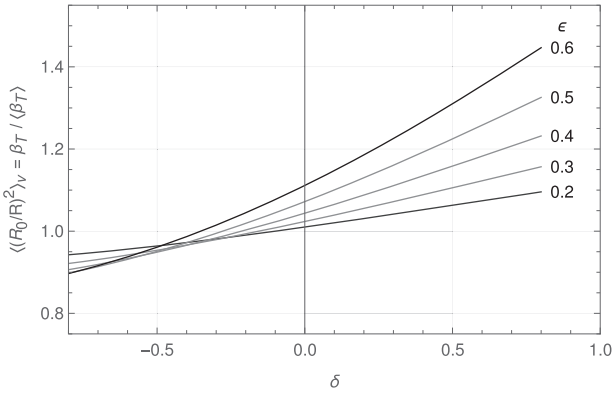

Figure 1. The effect of triangularity on $\langle p\rangle_V$ at fixed $\langle\beta_{N,v}\rangle$ for various inverse aspect ratios ϵ.

total energies. The two quantities β_T and $\langle\beta_T\rangle$ differ by a factor $\langle(R_0/R)^2\rangle_V$, which depends only on the shape of the LCFS—in our parameterization only on δ and the inverse aspect ratio $\epsilon = a/R_0$, but not on the elongation κ. Figure 1 shows the ratio $\beta_T/\langle\beta_T\rangle$, which reaches 40% for low aspect ratio and high triangularity. Similarly to Menard *et al* [2] we further define the three 'normalized beta' quantities

$$\beta_N = \beta_T \frac{aB_{T0}}{I_p}, \quad \langle\beta_N\rangle = \langle\beta\rangle \frac{aB_{T0}}{I_p}, \quad \text{and} \quad \langle\beta_{N,v}\rangle = \langle\beta_T\rangle \frac{aB_{T0}}{I_p}, \tag{7}$$

with total plasma current I_p in MA, minor radius a in m, and B_{T0} in T. Limits to MHD stability, in particular the Troyon limit [37], are conventionally defined in terms of β_N. However, Menard *et al* [2] found that when cast in terms of the second quantity, stability limits were nearly invariant with aspect ratio. The third is, again, used for the tokamak model in this paper because it does not rely on the specifics of a plasma equilibrium, and is typically only about 1% larger than the second. Like β_T and $\langle\beta_T\rangle$, β_N and $\langle\beta_{N,v}\rangle$ are simply related by the factor $\langle(R_0/R)^2\rangle_V$.

The geometric effect described here is that β_T and therefore $\langle p\rangle_V$ will decrease due to the lower value of $\langle(R_0/R)^2\rangle_V$ if either $\langle\beta_T\rangle$ is constant with triangularity or, equivalently, if $\langle\beta_{N,v}\rangle$ and I_p are constant with triangularity. We consider a constant $\langle\beta_{N,v}\rangle$ to be more natural than a constant β_N: in systematic stability scans [2], the maximum stable $\langle\beta_N\rangle$ was found to be nearly invariant with aspect ratio (for a fixed κ, δ, and bootstrap current fraction), while the corresponding β_T, $\langle\beta\rangle$, and β_N vary strongly with aspect ratio. However, we find that the maximum stable $\langle\beta_N\rangle$ is not quite invariant with triangularity; it decreases at low and very high δ. This 'physics effect' is described in section 3.2.3.

3.2.2. Geometric effect of strike point radius on peak heat flux and reactor availability. Another geometric effect is the radius of the outer strike point. This study assumes a conventional divertor geometry, with the outer strike point radius taken to be

$$R_{osp} = R_0 + a/4 - \delta a. \tag{8}$$

This ranges from $R_0 - a/2$ at $\delta = 0.75$ to $R_0 + a$ at $\delta = -0.75$. The strike point radius affects the scheduled downtime and availability of the reactor, f_{av}, as follows. The peak heat flux q_{div}, calculated using the heuristic drift model [38], decreases as R_{osp}^{-1}. In this calculation, we assume that the total angle at which field lines approach the divertor target, B_θ/B, is a fixed value imposed by the limitations of tile alignment [39]. Then the divertor target flux expansion [40]

$$\frac{R_{omp}B_{\theta,omp}}{R_{osp}B_{\theta,osp}} \propto \frac{R_{omp}B_{\theta,omp}}{R_{osp}(1/R_{osp})}, \tag{9}$$

is independent of R_{osp} and therefore independent of δ.

The divertors are assumed to have a useful lifetime of $F_{tt} = 10$ MW yr m^{-2} before they must be replaced [25], and the replacement time is assumed to be $t_{repl} = 180$ days [41]. For simplicity, and to maximize the effect of changing R_{osp}, the time required for blanket replacement and other maintenance is not considered. Thus availability is

$$f_{av} = (F_{tt}/q_{div})/(F_{tt}/q_{div} + t_{repl}). \tag{10}$$

Since the negative triangularity geometry allows a larger R_{osp}, then for the same P_{SOL}, the plasma-wetted area is larger, the peak heat flux q_{div} will be decreased, and the divertor modules can survive longer before replacement.

The assumption of a conventional divertor geometry is meant to be the simplest possible, and it is not clear that a conventional divertor is feasible for a fusion power plant. Solutions with more complicated magnetic geometries, such as the Super-X [42], or physical geometries, such as the vapor-box [43], would require a more sophisticated model.

If a large flux expansion is more difficult for negative triangularity machines, for example due to limited outboard space, the divertor challenge would rise inversely with the smaller flux expansion. A detailed study of the divertor magnetic configuration and coil placement would be required to ascertain how the flux expansion achievable at negative triangularity compares to that achievable at positive triangularity. Such a study is beyond the scope of this paper.

3.2.3. Physics effect of triangularity on $\langle\beta_{N,v}\rangle$. The two implemented physics effects of triangularity are a variation of the maximum stable $\langle\beta_{N,v}\rangle$ and an enhancement in the bootstrap current fraction. Menard's studies of ideal no-wall stability limits [2] using the DCON code [44] suggest that the maximum stable $\langle\beta_N\rangle$ is nearly constant with aspect ratio (from $\epsilon = 1.25$ to 10) at fixed κ, δ, and f_{BS}. However, there were not previously data on maximum stable $\langle\beta_N\rangle$ at fixed A, κ, and f_{BS} over wide ranges of δ, so a study using ideal MHD equilibrium and stability codes was undertaken, described in the appendix. We find that for the DEMO2 aspect ratio and elongation, the maximum stable no-wall $\langle\beta_N\rangle$ decreases from about 4.3 at $\delta = 0.5$ to 3.5 at $\delta = -0.5$. As shown in section 4, this effect of triangularity is larger than the others, so it should be given additional scrutiny. In particular, since trapped particle effects not captured in ideal MHD are expected to be

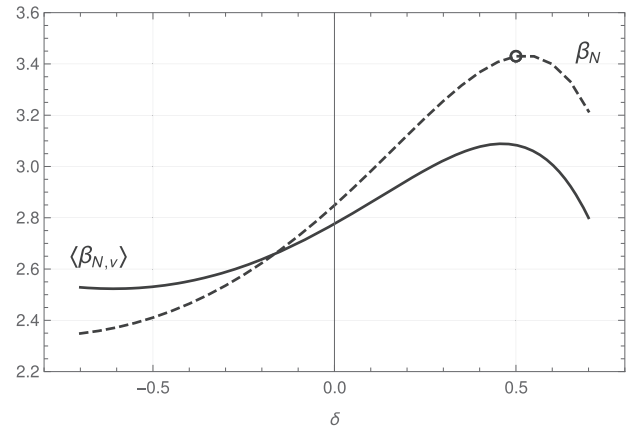

Figure 2. Maximum stable no-wall $\langle\beta_{\mathrm{N},v}\rangle$ and associated β_{N} for the DEMO2 shape parameters $A = 3.18$ and $\kappa = 1.8$ as a function of triangularity, scaled to match the β_{N} of the DEMO2 reference case (small circle). See appendix for details.

important for stabilizing negative triangularity tokamaks [45], further studies of stability limits should be undertaken.

Figure 2 shows the calculated $\langle\beta_{\mathrm{N}}\rangle$ and associated β_{N} as a function of δ which are used in the studies in sections 4 and 5. They have been scaled to match the DEMO2 reference case. In the FAROES model, the calculated $\langle\beta_{\mathrm{N}}\rangle$ is identified with a $\langle\beta_{\mathrm{N},v}\rangle$.

3.2.4. Physics effect of triangularity on bootstrap current fraction. The last major effect of δ is on f_{BS}, the fraction of the plasma current driven by the bootstrap effect. FAROES works with volume-averaged quantities and does not define radial profiles of density, temperature, or current, so f_{BS} is computed using a simplified formula. It is computed as

$$f_{\mathrm{BS}} = f_{\mathrm{f}} f_{\delta}\, 0.9\epsilon^{1/2}\beta_{\mathrm{p,th}}\ \max\left(1.2 - (q^*/11), 0.6\right), \qquad (11)$$

where q^* is the cylindrical safety factor [46],

$$q^* = \frac{L_{\mathrm{pol}}^2 B_{\mathrm{T0}}}{2\pi R_0 \mu_0 I}, \qquad (12)$$

$\beta_{\mathrm{p,th}}$ is the poloidal beta due to thermal particles, f_{δ} is a factor which adjusts the bootstrap current fraction to account for triangularity, and f_{f} is a 'supplementary factor', normally unity, which can be adjusted to match a more sophisticated point calculation. Aside from f_{f} and f_{δ}, equation (11) is similar to the 'ITER group' approximation in Wilson [47]. The factor f_{δ} captures the bootstrap fraction's proportionality to $f_{\mathrm{t}}/(1 - f_{\mathrm{t}})$ [48] where f_{t} is the fraction of trapped particles on a flux surface. Sauter [36] provides estimates for f_{t} as a function of ϵ and δ,

$$f_{\mathrm{t}} = 1 - \frac{1 - \epsilon_{\mathrm{eff}}}{1 + 2\sqrt{\epsilon_{\mathrm{eff}}}}\sqrt{\frac{1-\epsilon}{1+\epsilon}}$$

$$\epsilon_{\mathrm{eff}} = 0.67(1 - 1.4\delta\,|\delta|)\epsilon.$$

In FAROES, a 'typical' f_{t} is evaluated at a $\rho = 0.75$ flux surface, where δ_{75} is estimated to be half of the LCFS value δ. The

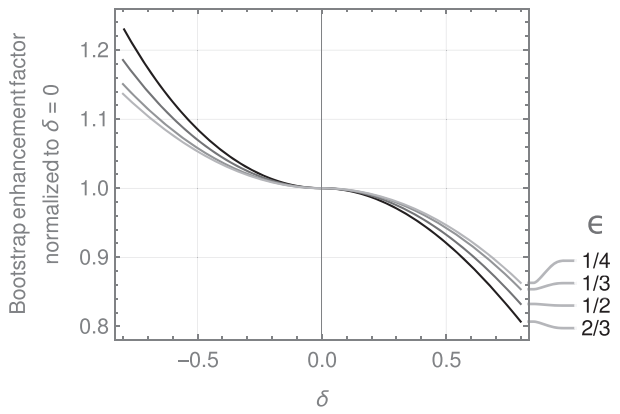

Figure 3. The bootstrap enhancement factor $f_{\delta} \propto f_{\mathrm{t}}/(1 - f_{\mathrm{t}})$ normalized to unity at $\delta = 0$.

Table 1. Parameters of the DEMO2 reactor computed by SYCOMORE [33] and FAROES. For FAROES, those in the first block are fixed, unless specified otherwise. Those in the middle block have been tuned using adjustment factors so that they match the $\delta = 0.5$ reference case; unless specified otherwise, their *factors* are then fixed and the values are recomputed self-consistently for other cases. Those in the last block result.

	SYCOMORE	FAROES
R/ m	8.46	8.46
a/ m	2.66	2.66
B_{t}/ T	5.53	5.53
f_{GW}	1.2	1.2
Z_{eff}	2.73	2.73
P_{NBI}/ MW	143	143
β_{N}	3.43	3.43
I_{p}/ MA	15.69	15.69
f_{BS}	0.41	0.41
q_{div}/ MW m^{-2}	10	10.0
H_{98}	1.4	1.4
$\langle n_{\mathrm{He}}\rangle_V/\langle n_{\mathrm{e}}\rangle_V$	0.073	n/a
$\langle n_{\mathrm{Ar}}\rangle_V/\langle n_{\mathrm{e}}\rangle_V$	0.0052	0.0056
τ_{E}/ s	3.55	3.76
$\langle n_{\mathrm{e}}\rangle_V/10^{20}$ m^3	0.794	0.847
$\langle T_{\mathrm{e}}\rangle_V$ /keV	15.16	15.42
P_{fus}/MW	1734	1937
Q_{phys}	12.52	13.54
P_{net}/MW	496	709

factor f_{δ} is normalized to unity for $\delta = 0$. Figure 3 plots f_{δ} for various ϵ. The term's deviation from unity grows quadratically with δ.

The lack of explicit profiles, or even representations of distinct H-mode and L-mode characteristics, necessitates this approach, which is heavily simplified compared to a full calculation of the bootstrap current. Additionally, the formula chosen neglects the greater contribution to bootstrap current from density gradients than from temperature gradients—this has substantial impacts on the optimal system, as shown by Buttery *et al* [49]. Finally, note that the effect of a larger bootstrap

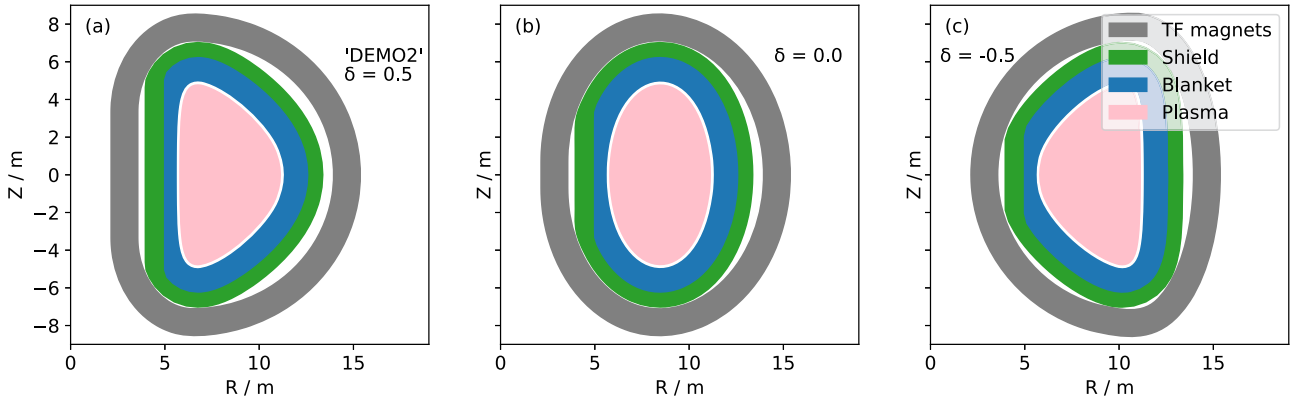

Figure 4. Three DEMO2-like reactors. Their inboard radial builds are matched to the steady-state DEMO2 reactor described by Reux [33].

fraction at negative triangularity has not yet been conclusively shown in experiments.

3.2.5. Physics effects of triangularity not included in the model. As the model lacks explicit profiles, or even differentiation between the H-mode and L-mode profiles associated with positive and negative δ, respectively, a number of important effects are neglected. This includes variations in fusion power, turbulence and confinement, current drive efficiency, energetic particle resonances, density limits, the relationship between the bootstrap current and dissipation, and differences in the requirements for divertor solutions. Negative triangularity plasmas may potentially operate with a lower P_{SOL} as in L mode they are not constrained to remain above the $P_{\mathrm{H}\to\mathrm{L}}$ threshold; this could simplify divertor power handling. We have not attempted to estimate or bound the magnitudes of the above effects, but we estimate the effect of the lack of a Shafranov shift, described below.

The model lacks a Shafranov shift. In the MHD equilibria studies described in the appendix, the Shafranov shift for the highest-$\langle\beta_{\mathrm{N}}\rangle$ negative and positive triangularity equilibria were 6% and 3%, respectively. A larger Shafranov shift increases the volume of the hot core plasma, and hence the fusion power. However, the FAROES tokamak model used here does not include a Shafranov shift; the radius of the magnetic axis is considered to be the same as that of the geometric center. Neglecting this effect causes a relative decrease in fusion power by a few percent in negative-triangularity cases, but this is much smaller than the decrease due to lower $\langle\beta_{\mathrm{N}}\rangle$.

4. DEMO2 reactors with varying triangularity and fixed toroidal field strength

For this study, we take a steady-state DEMO2 reactor modeled using the code SYCOMORE in a study by Reux [33] and build a comparable device using a FAROES tokamak model. In particular, it has the same radial build, elongation, B_{T0}, Greenwald fraction, and β_{N}. The DEMO reactor is chosen because it the target of other optimization studies, and this particular instance of DEMO2 was chosen for its well-defined radial build.

Its properties are summarized in table 1. Not all the parameters can be matched exactly; in particular, the current drive efficiency, bootstrap current, SOL width, and total thermal fusion power are tuned using adjustment factors of order unity to match $I_{\mathrm{p}} = 15.69$ MA, $f_{\mathrm{BS}} = 0.41$, $q_{\mathrm{div}} = 10$ MW m^{-2}, and $H_{98} = 1.4$. Note that the adjustment tuning is performed for the $\delta = 0.5$ reference case; the adjustment factors are not changed again and when running the other cases described in section 4.1 the quantities I_{p}, f_{BS}, q_{div}, H_{98}, and τ_{E} are outputs of the solver. No explicit confinement assumption is necessary; instead, confinement is implicitly defined by the combination of plasma geometry, f_{GW}, $\langle\beta_{\mathrm{N}}\rangle$, Z_{eff}, and the need to both heat and drive current solely via the neutral beams with power P_{NBI}.

For the $\delta = 0.5$ case, the fusion power and net electric power are each larger by about 200 MW, and $\langle n_{\mathrm{e}}\rangle_V$ and $\langle T_{\mathrm{e}}\rangle_V$ are similar. The thermal efficiency and NBI wall plug efficiency are not specified explicitly by Reux, but values of 0.52 for each are consistent with the net electric power produced; this implies a recirculating power fraction f_{recirc} of 0.31. The FAROES runs in this study use a thermal efficiency of 0.5 and NBI wall-plug efficiency of 0.5, so f_{recirc} is 0.38.

We have not attempted to exactly reproduce the SYCOMORE DEMO2 and there are important differences in the models. One is that the present FAROES model does not account for any He ash concentration. Another is that the particular plasma volumes, surface areas, and poloidal circumferences are also different between the two models: the helios [50] plasma module used by SYCOMORE describes plasma shapes with sharp X-points, while the present FAROES tokamak model has only smooth shapes. While differences in the models do lead to differences in fusion power and other values, this is not critical for the present study, which is concerned with trends rather than exact quantities.

A family of DEMO2-like reactors is studied with fixed radial build, magnetic field strength, plasma elongation, Z_{eff}, and f_{GW}, but with triangularity varying from $\delta = 0.7$ to $\delta = -0.7$. Figure 4 shows how the plasma, blanket, shield, and toroidal field coils deform as the triangularity changes. The shapes of inner and outer edges of the blanket and shield are parallel curves to the plasma shape. The inboard side is optionally modified by vertical cuts on the outer edges. This allows independently setting the inboard and outboard midplane thickness of each component. The inner profile of the toroidal field coils consists of a vertical segment on the inboard

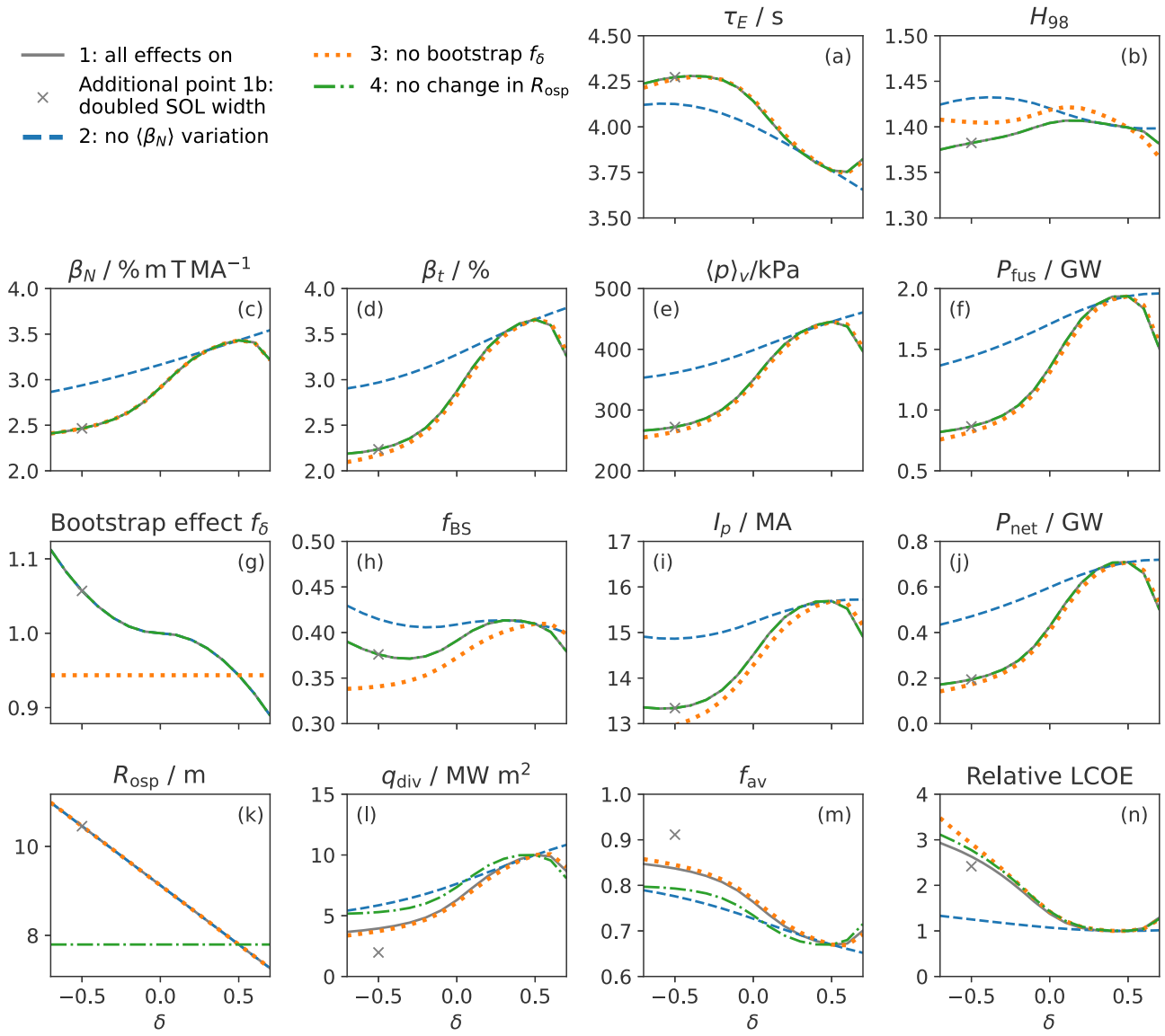

Figure 5. Results of four scans of triangularity, plus one additional point. The first is a 'standard' scan with all the studied effects of triangularity turned on. Scans 2, 3, and 4 knock out the effects of triangularity on $\langle\beta_N\rangle$, the bootstrap fraction (f_δ) and the strike point radius R_{osp}, respectively. The additional point, labeled 1b, has a doubled SOL layer width. Note that in some subplots, several curves are overlapping.

side, two quarter-circle arcs, and a half-ellipse arc on the outboard side. The outer profile curve is parallel to the inner profile, so that the magnet has a uniform thickness. For each δ, the magnet profile is fit around the shield to minimize the reactor's capital cost.

4.1. Overview of the studies in this section

Except where indicated otherwise, all the studies here hold fixed the six parameters in the top block of table 1. Subsection 4.2 presents an initial set of four scans. In the first, the triangularity of the reactor is varied, including all the effects described in section 3.2. The LCOE is computed for each reactor. In three more scans, three of the effects of triangularity are turned off, one at a time, to assess their contribution to the LCOE. It is shown that the decrease of β_N with decreasing δ strongly increases the LCOE. The increase of the bootstrap fraction factor f_δ and R_{osp} as δ decreases moderately lowers the cost, but not enough to compensate. These results are reported in detail below.

Subsection 4.3 shows that changes in the LCOE in the first four scans are not caused by the machine geometry itself impacting the capital cost.

In two further studies presented in subsection 4.4, $\langle\beta_{N,v}\rangle$ and the bootstrap current supplementary factor f_f are allowed to vary freely, to find the magnitude by which these parameters must be enhanced to keep the LCOE fixed as δ changes.

4.2. Changes in LCOE are driven by changes in physics

Figure 5 shows key results of the first four scans. In the standard scan 1, gray, the decreasing β_N as δ decreases leads to a lower β_T, lower ⟨p⟩$_V$, and a halving of the fusion power. The increase in f_δ competes with the lower $\beta_{p,th}$ to keep f_{BS}

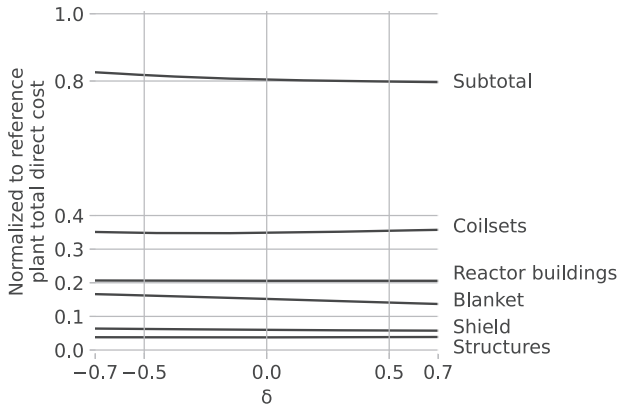

Figure 6. Changes in the largest direct capital costs [25] with triangularity due to changes in physical dimensions alone. These costs apply to all the DEMO2-like reactors. Costs which are functions of thermal or electric powers rather than volume are not shown; the subtotal is the sum of the five listed components.

similar, while the total I_p decreases despite the same current drive power. The increase in R_{osp} and the decreased P_{fus} lead to a 60% smaller q_{div}, which allows a longer time between divertor replacements and increased availability. However, effects of the higher bootstrap fraction and availability are overshadowed by the decreased fusion power; the lower power out from a device of the same dimensions leads to the LCOE rising to 262% of the reference case value at $\delta = -0.5$.

In scan 2, shown with blue dashed lines, the MHD stability limit's variation with δ is ignored, so $\langle\beta_{N,v}\rangle$ is a constant as δ is scanned. Even without this effect, the LCOE increases as δ and β_N decrease. This suggests that unless $\langle\beta_N\rangle$ can somehow be increased for negative triangularity reactors, their lower volume-averaged pressure will be a major penalty to their economics.

In scan 3, shown with orange dotted lines, the term f_δ in equation (11) is fixed to its value at $\delta = 0.5$. Compared with scan 1, this leads to a lower f_{BS} and lower I_p, as well as slightly lower β_T, $\langle p\rangle_V$, and fusion power. The LCOE at $\delta = -0.5$ increases from 262% to 318% of the reference case value. This effect on cost is much smaller than that shown by scan 2, suggesting that in cases with an aspect ratio of around 3 and a modest f_{BS}, gains in bootstrap fraction due to a higher trapped particle fraction are not large enough to offset the losses of fusion power due to lower β_N.

In scan 4, green, the outer strike point radius is fixed. Compared with scan 1, this leads to a larger q_{div}, and the availability (assumed to be driven by periodic divertor replacement) decreases from 0.84 to 0.79. This leads to an increase in the LCOE from 262% to 277% of the reference case value at $\delta = -0.5$. This shows that, at least for the assumed 10 MW yr m^{-2} divertor lifetime and replacement time of 180 days, the increase in strike point radius with negative triangularity does not substantially decrease the cost. Of course, this analysis neglects the possibility of a threshold peak heat flux below which a given divertor technology becomes feasible. It also does not capture the distinction between ELMing and ELM-free plasmas. Without an ELM-free plasma regime, as has been demonstrated in negative triangularity [17], divertor power handling may be much more difficult or even intractable.

One additional point, labeled 1b, was also run. This point has the characteristics of those in scan 1 except for a doubled SOL width, to represent the larger SOL width typical of L-mode plasmas. Due to the lower divertor heat flux, the availability rises to 0.91 and the LCOE drops to 242% of the reference case value, still much higher than the baseline $\delta = 0.5$ configuration cost.

Overall, with the assumed variation in $\langle\beta_{N,v}\rangle$ with δ, the lower β_N at negative triangularity leads to a lower fusion power and much higher costs of electricity. The larger bootstrap current and strike point radii improve the economics, but not enough to make up for the loss of β_N.

4.3. Changes in tokamak core capital cost at fixed *R*, *a*, κ

The costing of the tokamaks follow Sheffield's formulation [25, 51]. While some components (such as the electricity generation systems) are costed according to their rated power, the coils, blankets, shield, and reactor buildings are costed using functions of their volume. Since the radial build (including R and a) and elongation are fixed in this study, the costs of those in the second category vary only slightly with triangularity. As shown in figure 6, the subtotal cost of these components increases less than 3% as triangularity is decreased from $\delta = 0.5$ to $\delta = -0.5$. Therefore, within this framework, overall costs of electricity are driven by the changes in reactor physics, as described in the prior section, more than they are driven by changes in the physical machine shape. The next subsection examines what improvements to reactor physics—$\langle\beta_N\rangle$ or f_{BS}—would be necessary to keep costs fixed as triangularity is changed.

4.4. Required improvements in physics for equal costs

Two further studies are performed to determine the factors by which $\langle\beta_N\rangle$ or f_{BS} would need to improve with negative triangularity in order to keep the LCOE fixed.

It may be possible to increase $\langle\beta_N\rangle$ by adding conducting elements near the plasma, using feedback mechanisms [52], altering current profiles, or employing plasma rotation or rotational shear [2]. Figure 7 shows a collection of scans, five with fixed $\langle\beta_{N,v}\rangle$, and one (dashed) with the quantity allowed to vary in order to keep the LCOE fixed. The value of $\langle\beta_{N,v}\rangle$ at $\delta = -0.5$ must increase to 3.4, 10% higher that at $\delta = 0.5$, to keep the same cost of electricity. This enhancement of $\langle\beta_{N,v}\rangle$ largely counteracts the falling $\langle(R_0/R)^2\rangle_V$ and allows the fusion power to be kept nearly constant, leading to constant net power generation. However, this presumed effect is contrasted by the 18% decrease in the maximum stable $\langle\beta_N\rangle$ found by the stability studies, which leads to a $\langle\beta_{N,v}\rangle$ of 2.65.

Alternately, it may be possible to increase the bootstrap current by carefully controlling profiles of density and 'seed current'. Figure 8 shows the results of five scans of triangularity: four (solid lines) have different fixed bootstrap current supplementary factors f_f and P_{NBI} is allowed to vary to keep $H_{98} = 1.4$, and one (dashed black line) allows both f_f and P_{NBI} to vary in order to keep both LCOE and H_{98} fixed. These

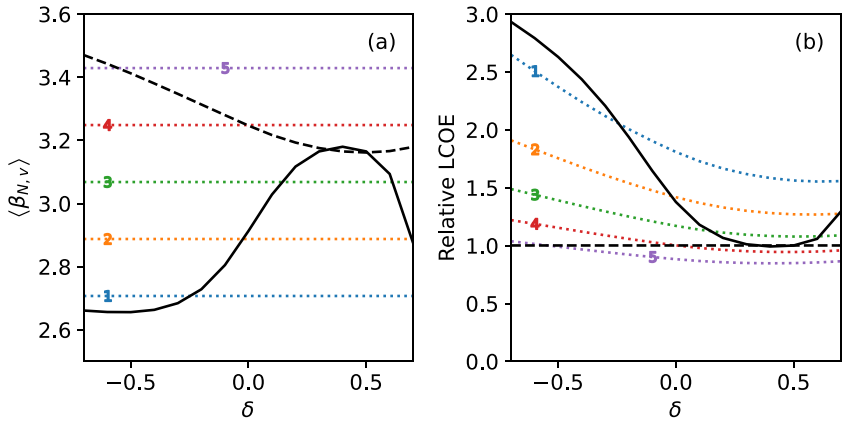

Figure 7. Seven scans of δ: five with $\langle\beta_{\mathrm{N},v}\rangle$ fixed at various levels (colored solutions, labeled 1-5), one with variation proportional to the stability limits found by the MHD codes (black), and one with it allowed to vary so that the LCOE is constant (dashed). To keep the LCOE constant, $\langle\beta_{\mathrm{N},v}\rangle$ must be 10% higher at $\delta = -0.5$ than at $\delta = 0.5$, rather than the 18% lower found in our stability studies.

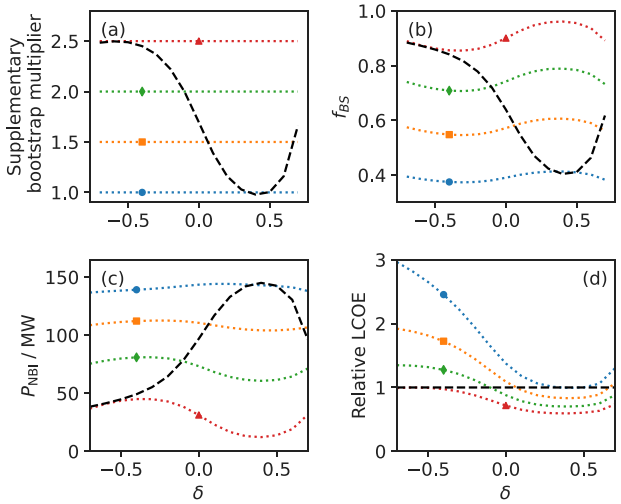

Figure 8. Five scans of triangularity studying the changes that supplementary factors (*a*) to the bootstrap fraction (*b*) formula have on the LCOE (*d*). Four scans (dotted, identified by shapes) have fixed supplementary factors of 1.0 to 2.5×, and one (dashed black line) in which the supplementary factor is varied in order to keep LCOE fixed. In each scan, the neutral beam power, (*c*), is allowed to vary to keep a constant $H_{98} = 1.4$. The bootstrap current fraction must increase substantially, from 41% at $\delta = 0.5$ to 86% at $\delta = -0.5$, to keep the LCOE constant.

scans show that at fixed H_{98}, a negative triangularity tokamak requires a significantly higher bootstrap fraction—an increase from 41% to 86%—to yield the same LCOE. A higher f_{BS} requires less neutral beam current drive, which allows higher net electric power and so higher revenue. To keep the LCOE fixed, the $\delta = -0.5$ machine requires a 2.5× increase in f_{f} over the $\delta = 0.5$ machine, even after including f_δ, the effect expected from the higher trapped particle fraction. The change in required bootstrap fraction is a 1.85× increase rather than 2.5× because other factors in equation (11) have decreased.

We have shown that at constant B_{T0} and f_{GW}, the negative triangularity DEMO2 could employ substantial increases in either $\langle\beta_{\mathrm{N}}\rangle$ or f_{BS} to reach LCOE parity with the positive-triangularity reference case. Alternately, other methods, such as improved profiles, confinement, current drive efficiency, or magnetic field strength could potentially be employed, especially in combination. In the next section we study the necessary increase in B_{T0} to reach LCOE parity for the negative triangularity machine; the other potential methods are not examined in this study.

5. The high-field path to practical negative triangularity reactors

Advances in high-temperature superconducting magnet technology [23] may prove especially beneficial to negative-triangularity reactors [19]. Despite the lower achievable β_{N}, negative-δ reactors can still reach adequate fusion performance with increased toroidal field, while keeping divertor heat fluxes below those of positive-δ machines. Depending on the costs of the magnets, this may even lead to a LCOE which is superior to that of positive-δ reactors. Thus, if reactors are limited by divertor technology and not by magnet technology, a negative-δ reactor may be the best solution. We find the minimum field strengths to match the LCOE and the peak divertor heat flux of the reference positive-δ DEMO2. These are 7.2 T and 9.2 T, respectively, versus 5.53 T for the reference case. We also discuss the challenges of engineering magnets for negative-δ reactors.

5.1. Required magnet engineering enhancements to equalize costs and divertor heat fluxes

Machines at $\delta = -0.5$ with field strengths increased to 7.2 T to 9.18 T will have both lower LCOE and lower peak heat flux q_{div} than the reference DEMO2 machine. A set of scans of triangularity was carried out with the toroidal field, B_{T0}, as a design variable and a LCOE value as a constraint. This finds the required B_{T0} to yield a certain LCOE as a function of triangularity.

In figure 9, the results of these scans are plotted in the space of B_{T0} and the peak divertor heat flux q_{div}. The DEMO2 reference case is marked with a dot. This map shows that if B_{T0} can be increased, there is a region where a negative-triangularity reactor may have a lower peak heat flux *and* a lower LCOE than the reference case. This region is above the '1.0×' cost contour and to the left of the $q_{\mathrm{div}} = 10$ MW m^{-2} tick. Table 2 details specific points within this region, at $\delta = -0.5$. An

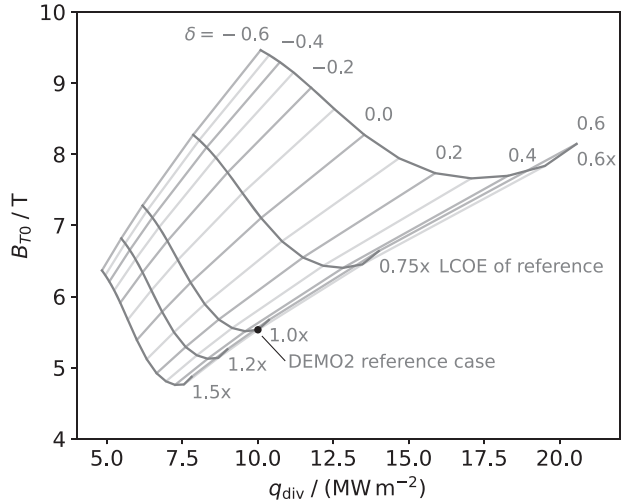

Figure 9. Map of the required B_{T0} and resulting peak heat flux q_{div} to keep a fixed LCOE as δ is varied. The LCOE values of each contour are labeled as factors of that of the B_{T0}, $\delta = 0.5$ reference case, which is marked with a dot.

Table 2. Changes in LCOE and divertor heat flux when varying B_{T0} by factors m at $\delta = -0.5$. Compare to the 10 MW m^{-2}, $\delta = 0.5$ reference machine with $B_{T0} = 5.53$ T in table 1.

m	B_{T0} (T)	P_{fus} (GW)	P_{net} (GW)	Relative LCOE	q_{div} (MW m^{-2})
1.3	7.20	1.755	0.621	1.01	6.3
1.66	9.18	3.191	1.311	0.62	10.0

increase to 7.2 T, 1.3 times its original value of 5.53 T, matches the LCOE of the $\delta = 0.5$ machine. Thus, a higher B_{T0} compensates for the lower β_N achievable at $\delta = -0.5$. Additionally, due to the larger outer strike point radius, the heat flux there is 6.3 MW m^{-2}, 63% of that of the base $\delta = 0.5$ design. Increasing the field strength to 9.18 T matches the outer divertor heat flux of 10 MW m^{-2} and further lowers the LCOE to 62% of that of the reference case.

These calculated increases in B_{T0} are minimum values: they do not account for increasing costs of the magnets themselves as the field strength is increased. In the Sheffield costing model [25], used in FAROES for this study, the magnets are priced only according to their material volume, not the field that they generate, shape, or other characteristics that affect the difficulty of engineering and fabrication. The values calculated here also do not consider additional magnet width or height required to manage the toroidal field ripple (see below). The changes in LCOE with B_{T0} will then be smaller than those reported here. Hence, the required B_{T0} to reach LCOE parity will be higher.

Similarly, one could expect that a divertor engineered to handle a higher peak heat flux will be more expensive than one required to handle a lower heat flux. Thus, a more accurate map would be stretched both horizontally and vertically compared to this one.

5.2. Magnet engineering considerations for negative-δ reactors

As shown above, in order to reach the same LCOE, the toroidal field magnets for negative-δ reactors will need to generate stronger fields than those of positive-δ reactors. There are further reasons they may cost more than those for positive-δ reactors. First, their engineering may be more difficult due to their shape. Second, they may need to be built wider or taller in order to reach acceptable levels of fast-particle losses due to toroidal field ripple, which given the same magnets may be larger in plasmas with negative-δ shaping.

As noted above, the magnet cost model used in this paper is simplistic, so the changes in costing due to the remedies discussed in this section are meant only to be rough indications of magnitudes and direction. More sophisticated magnet cost models should be introduced.

5.2.1. Difficulties due to magnet shape. Toroidal field magnets for existing and proposed future tokamaks generally approximate the constant-tension 'Princeton D' shape [53] by incorporating a larger radius of curvature at larger R. One might therefore expect that a substantial deviation from this profile, such as the 'picture frame' magnets depicted by Kikuchi *et al* [54], could increase the cost to achieve the same field, for example if more complicated support structures are required.

5.2.2. Negative triangularity may require wider or taller magnets to limit ripple transport. We find that enlargements to the magnets in order to limit toroidal field ripple for negative-triangularity tokamaks may increase the LCOE by a few percent. Toroidal field ripple arises from the gaps between magnet legs, especially on the outboard side. This variation in field strength causes ripple trapping and stochastic ripple banana-drift diffusion, which can cause alpha particles to be lost to the wall before thermalizing [32]. This deprives the plasma of some fraction of the alpha heating and leads to localized hot spots on the wall.

Codes like ASCOT and SPIRAL [55] trace particle orbits to calculate the ripple loss fraction for a plasma in a set of coils. However, these can require hundreds of CPU-hours per run [56], which is not suitable for a zero-D systems code. Instead, systems codes typically compute the ripple magnitude at the (midplane) plasma boundary and axis [57], which can be done in milliseconds. A typical maximum value for ripple at the LCFS is 0.6%, used for EU-DEMO studies [58]. Here, we conservatively extend the limit criterion to cover the whole LCFS, not just the midplane.

We compute the ripple using the toroidal field coil shapes for the $\delta = 0.5$ and $\delta = -0.5$ machines shown in figure 4. The current from each of the 18 magnets is computed using five parallel current filaments, identically shaped and stacked toroidally to approximate a ribbon of current with the toroidal width of the magnet's inboard leg. Each filament is divided into 200 straight current elements for the Biot–Savart law computation. The profile of the filaments aligns with the average winding pack radius.

Figure 10 visualizes ripple magnitude contours for the two machines. Despite the height of the magnet in (*a*) being the same height as in (*b*), corresponding ripple contours have smaller heights in the latter, and are shifted slightly outward at their peaks. The LCFS of the $\delta = 0.5$ machine slightly exceeds the 0.5% contour near the outboard midplane. If necessary,

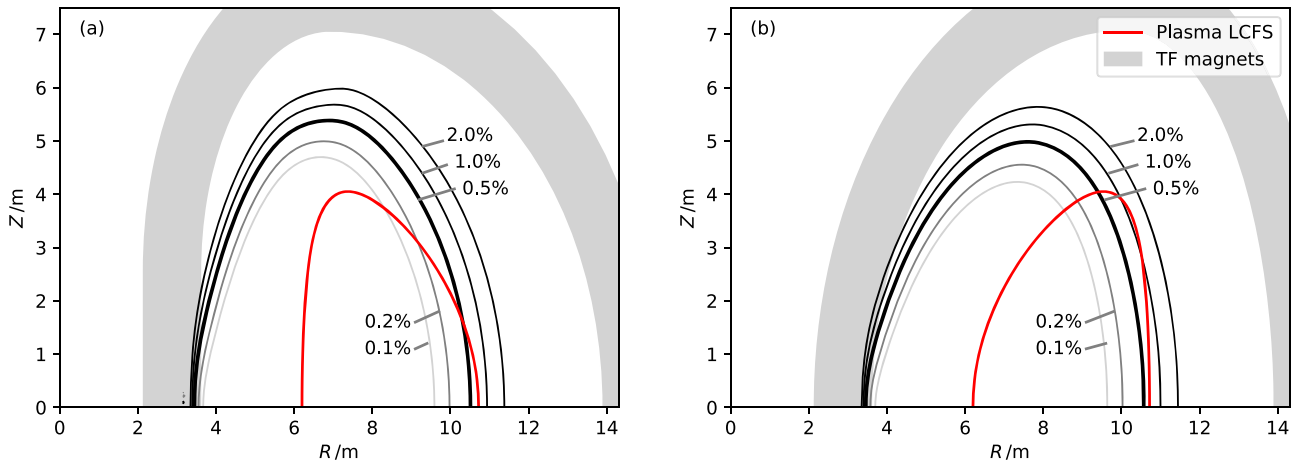

Figure 10. Contours of toroidal field ripple for the (*a*) $\delta = 0.5$ and (*b*) $\delta = -0.5$ DEMO2-like machines, with the magnet configurations as shown in figure 4. The 0.5% ripple contour is highlighted as it is a typical limiting value. At $\delta = -0.5$, the plasma exceeds the 0.5% contour over a large region near the *X*-point.

this can be corrected by increasing the outboard leg radius by 0.3 m, which increases the LCOE by about 0.8%. For the $\delta = -0.5$ machine, the LCFS exceeds the 1.0% ripple contour near the *X*-point. To maintain a ripple everywhere within the LCFS of less than 0.5%, the outboard leg can be moved outward by 1.1 m. This increases the LCOE by 3%.

The relative magnet cost increase for $\delta = -0.5$ would be higher if the LCFS ripple must be lower than 0.5%: since for the same magnet height, equivalent ripple contours peak at a lower Z value at negative δ, the magnet height as well as the outer leg radius may need to increase. However, it is a conservative assumption here that a plasma's ripple losses are defined by the largest ripple anywhere on the LCFS. It is expected that ripple near the *X*-point is less important for confinement than ripple near the midplane [56], so the necessary cost increase to achieve a low enough global fast particle loss fraction may not be so high. More detailed studies of ripple transport for negative-δ tokamaks should be performed.

6. Discussion

We have studied the impact of changing the triangularity of a steady-state DEMO2-like device using a novel open-source fusion reactor optimization framework, FAROES. As the model is zero-dimensional, it does not include variations in confinement physics or in profiles of densities and temperatures that are expected to occur with changes in triangularity. These changes would lead to further variations in fusion power, bootstrap current, pressure limits, radiated power, and other effects. The simplified nature of the model should be considered as context for this discussion.

In the steady-state DEMO2-like device, the base configuration with $\delta = 0.5$ has a moderate bootstrap current fraction of 0.41 and a relatively high recirculating electric power fraction of order 40%, which leaves little room for decreasing the fusion power. We first studied a scenario where the magnetic field is limited to its DEMO2 value of $B_{T0} = 5.53$ T. As we assume that MHD stability requirements limit reactors to a $\langle\beta_{N,v}\rangle$ which decreases as δ is decreased, the fusion power density of the plasma decreases as well. This leads to a lower net output power, a higher f_{recirc}, and large increase in the LCOE. One way to keep costs fixed would be to somehow *increase* $\langle\beta_{N,v}\rangle$ by about 10% for a negative triangularity machine, which is in contrast with the 18% reduction due to MHD limits found in this study. This being said, the MHD limit study performed for this work is simplistic, and the possibility of raising β limits through profile tailoring, wall stabilization, or other means is an interesting path to explore. There is some indication that wall stabilization may be less effective for negative triangularity shapes due to strong coupling between fixed-boundary global Mercier modes [31] or internal models [21] and external kink modes, and to reach similar β_N limits via stabilization a closer-fitting wall may be required [59].

Alternately, the cost could be held fixed if the bootstrap fraction can increase (to roughly 0.86) while P_{NBI} is reduced, which decreases the required recirculating power. The required increase in bootstrap fraction is much larger than that estimated by our simple model of f_δ, which gives an increase of about 12%; a *supplementary* multiplier of about 2.5 in the f_{BS} formula is needed to compensate. Current experimental evidence does not lend support to an enhancement of this magnitude in f_{BS} with negative triangularity. Possible enhancements to the bootstrap fraction at negative triangularity should be studied with more sophisticated models and experiments.

If the magnetic field is held fixed, then a shift from positive to negative triangularity will increase costs. However, if the tokamak is limited by divertor heat fluxes or ELMs and not by magnet engineering, a negative-triangularity solution could prove useful. A 30% higher toroidal field compensates for the lower β_N at $\delta = -0.5$, and yields a reactor with the same LCOE but with a 37% lower peak heat flux at the outer divertor than the base $\delta = 0.5$ case. A further decrease in target heat loads may be possible by operating in L-mode rather than H-mode. This, together with a lack of ELMs, would bring the divertor technology further within technological limits,

such that it might become economical to again increase power density despite larger peak heat fluxes.

Of course, increasing B_{T0} may be difficult: there is often already an incentive to maximize field strength for a given magnet radial footprint, as it yields a larger fusion power, and the geometry of negative triangularity may lead to more difficult and costly magnet engineering. As the magnets are costed purely by their material volume in this study, these increased costs are not accounted for. Additionally, there may be a need to increase magnet dimensions to limit the toroidal field ripple that causes fast-ion losses. However, the magnitude of these losses for negative-δ configurations has not been well-studied and is difficult to estimate; further research should be performed.

There are additional important caveats for this study. First, the cost model does not incorporate the price of ELM mitigation techniques which may be necessary for positive triangularity, but not necessary for negative triangularity. Second, the divertor lifetime model, which is linear with peak heat flux, is somewhat lacking. As heat fluxes are reduced away from their technological limits, it could be expected that less costly technology with lower complexity or larger margins could be employed.

7. Conclusion

Achieving a high-pressure, high-power-density plasma is essential for the economy of fusion reactors. We have examined the effects of a changing triangularity on a DEMO2-like tokamak using a heavily simplified model. As the model is essentially zero-dimensional, it ignores known effects of the shape on transport and MHD stability and therefore on profiles, bootstrap currents, radiation, and other physics that would be captured in a more sophisticated model. We have found that, at least within our simplified framework, negative-triangularity reactors suffer twice in the pursuit of a high-pressure plasma: once from the lower maximum stable $\langle\beta_{N,v}\rangle$ due to MHD, and again from the lower volume-averaged pressure $\langle p\rangle_V$ for a given $\langle\beta_{N,v}\rangle$ due to the fall-off of magnetic field strength as $1/R$. We find that despite increases to the bootstrap current fraction (due to a higher trapped particle fraction in the negative-triangularity flux surfaces) and availability (due to lower heat fluxes on the outer divertor), the decrease in fusion power due to lower β_N dominates the economics of the machine.

Especially if improvements to bootstrap currents, current drive efficiency, radiation limits, and confinement properties cannot be made by tailoring profiles, one possible way to remedy this would be to increase the toroidal field to compensate for the loss in β_N. We find that for a DEMO2-like steady state tokamak with $A = 3.18$ and $\kappa = 1.792$, the field strength must be increased from 5.53 T to 7.20 T to keep cost parity as triangularity is shifted from $\delta = 0.5$ to $\delta = -0.5$. If this is possible, then while assuming fixed profiles and similar H_{98}, the negative-δ reactor can achieve similar fusion power but with significantly lower outboard divertor heat loads. Thus, if reactors are limited by divertor engineering more strongly than they are limited by magnet engineering, the negative triangularity reactor may be the more economical solution. This being said, the study should be repeated with more sophisticated physics and engineering models, especially involving self-consistent profiles, current drive, and bootstrap current calculations.

Acknowledgments

Thanks to J. Menard for the early modeling work which became FAROES; Rory Conlin, Yueqiang Liu, Zhirui Wang, and Olivier Sauter for help with CHEASE; Alex Glasser for help with DCON; Gerrit Kramer for discussion of the effects of magnetic field ripple; and Charles Swanson, Walter Guttenfelder, Carlos Paz-Soldan, and Menard for reviews of early drafts. This work was supported by the US Department of Energy under Contract Number DE-AC02-09CH11466. The United States Government retains a non-exclusive, paid-up, irrevocable, world-wide license to publish or reproduce the published form of this manuscript, or allow others to do so, for United States Government purposes.

Data availability statement

Data for this paper are archived at http://arks.princeton.edu/ark:/88435/dsp01rf55zb85t.

Appendix. Maximizing the normalized beta

This appendix describes the calculation of a maximum ideal, no-wall $\langle\beta_N\rangle$ as a function of δ. The Grad–Shafranov solver CHEASE was used to generate equilibria with the same A and κ as the DEMO2 reactor above and with δ from -0.9 to 0.9. The plasma boundary shape is that of equation (2). The pressure profiles and current-like profiles are simple functions,

$$p = p_0(1 - \hat{\psi}^{b_{p1}})^{a_{p1}}, \tag{13}$$

$$\frac{\langle \mathbf{J}\cdot\mathbf{B}\rangle}{\langle \mathbf{B}\cdot\nabla\phi\rangle} \propto (1 - \hat{\psi}^{b_{c1}})^{a_{c1}}, \tag{14}$$

and are a subset of the family in Menard *et al* [2]. Note that the FAROES tokamak model used in this paper is zero-D and these profiles are used only by the MHD codes.

An optimization procedure was used to find, for each δ, the profiles with the highest $\langle\beta_N\rangle$ that are stable to no-wall free-boundary and fixed-boundary modes and which have bootstrap fractions from 40% to 55%. Equilibria with local bootstrap current 'overdrive' (a local bootstrap current density larger than the total current density) were not screened out; this may be the reason for the relatively high $\langle\beta_N\rangle$ limits found here, and future studies should consider screening for this effect. Stability was assessed using DCON [44], for toroidal mode numbers $n = 1$, 2, and 3. For each pair of profile functions plus a central safety factor q_0 (chosen to be in [1.02, 1.4]), the maximum stable p_0 is found. This maximizes $\langle\beta_N\rangle$.

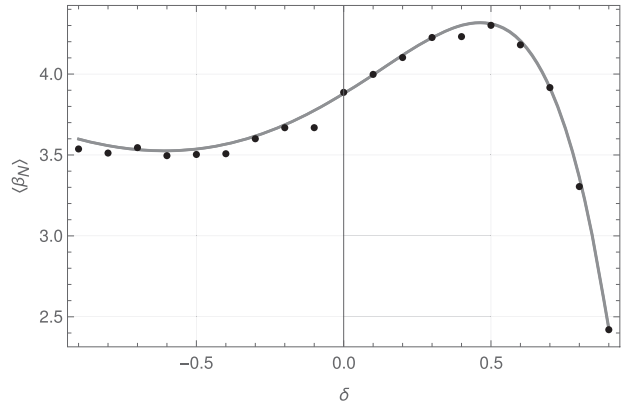

Figure 11. The stable equilibria with the highest $\langle\beta_N\rangle$ and acceptable f_{BS} at each value of δ. The gray line is a fit from a ratio of third and second-degree polynomials.

As a first round, a random sample of 400 profiles were evaluated for each δ. A Bayesian Gaussian process optimizer [60] was used to determine additional sets of points to run in fifteen subsequent parallel rounds. The top $\langle\beta_N\rangle$ for each δ are shown in figure 11. We find that the maximum stable $\langle\beta_N\rangle$ decreases by about 18%, from 4.3 to 3.5, as δ goes from 0.4 to −0.6. A ratio of two polynomials is fit to the data to form a smooth function of δ.

As noted in section 3.2.1, the $\langle\beta_N\rangle$ maximized here is not the same as $\langle\beta_{N,v}\rangle$ which used in the FAROES tokamak model; for the best stable equilibria the latter is about 1% larger than the former.

ORCID iDs

J.A. Schwartz https://orcid.org/0000-0001-9636-8181
A.O. Nelson https://orcid.org/0000-0002-9612-1936
E. Kolemen https://orcid.org/0000-0003-4212-3247

References

[1] Kikuchi M. 1993 Prospects of a stationary tokamak reactor *Plasma Phys. Control. Fusion* **35** B39–53
[2] Menard J.E. *et al* (NSTX National Research Team) 2004 Aspect ratio scaling of ideal no-wall stability limits in high bootstrap fraction tokamak plasmas *Phys. Plasmas* **11** 639–46
[3] Freidberg J.P., Cerfon A. and Lee J.P. 2015 Tokamak elongation—how much is too much: I. Theory *J. Plasma Phys.* **81** 515810607
[4] Lee J.P., Cerfon A., Freidberg J.P. and Greenwald M. 2015 Tokamak elongation—how much is too much: II. Numerical results *J. Plasma Phys.* **81** 515810608
[5] Najmabadi F. 2003 Spherical torus concept as power plants-the ARIES-ST study *Fusion Eng. Des.* **65** 143–64
[6] Menard J.E. *et al* 2016 Fusion nuclear science facilities and pilot plants based on the spherical tokamak *Nucl. Fusion* **56** 106023
[7] Lazarus E.A., Hyatt A.W. and Osborne T.H. 1994 The role of shaping in achieving high performance in DIII-D *15th Int. Conf. on Plasma Physics and Controlled Nuclear Fusion* (Madrid, Spain October 1994)
[8] Shimada M. *et al* 2007 Progress in the ITER Physics Basis, Chapter 1: Overview and summary *Nucl. Fusion* **47** S1
[9] Wagner F. 2007 A quarter-century of H-mode studies *Plasma Phys. Control. Fusion* **49** B1
[10] Zohm H. 1996 Edge localized modes (ELMs) *Plasma Phys. Control. Fusion* **38** 105–28
[11] Leonard A.W. 2014 Edge-localized-modes in tokamaks *Phys. Plasmas* **21** 090501
[12] Viezzer E. 2018 Access and sustainment of naturally ELM-free and small-ELM regimes *Nucl. Fusion* **58** 115002
[13] Paz-Soldan C. 2021 Plasma performance and operational space without ELMs in DIII-D *Plasma Phys. Control. Fusion* **63** 083001
[14] Evans T.E. 2013 ELM mitigation techniques *J. Nucl. Mater.* **438** S11–8
[15] Loarte A. *et al* 2014 Progress on the application of ELM control schemes to ITER scenarios from the non-active phase to DT operation *Nucl. Fusion* **54** 033007
[16] Gunn J.P. *et al* 2017 Surface heat loads on the ITER divertor vertical targets *Nucl. Fusion* **57** 046025
[17] Austin M.E. *et al* 2019 Achievement of reactor-relevant performance in negative triangularity shape in the DIII-D tokamak *Phys. Rev. Lett.* **122** 115001
[18] Marinoni A. *et al* (DIII-D Team) 2019 H-mode grade confinement in L-mode edge plasmas at negative triangularity on DIII-D *Phys. Plasmas* **26** 042515
[19] Kikuchi M. *et al* 2019 L-mode-edge negative triangularity tokamak reactor *Nucl. Fusion* **59** 056017
[20] Kikuchi M., Takizuka T. and Furukawa M. 2014 Negative triangularity as a possible tokamak scenario *12th Asia Pacific Physics Conf. (APPC12)* (Chiba, Japan July 14–19, 2013) **1** 015014
[21] Medvedev S.Y. *et al* 2015 The negative triangularity tokamak: stability limits and prospects as a fusion energy system *Nucl. Fusion* **55** 063013
[22] Marinoni A., Sauter O. and Coda S. 2021 A brief history of negative triangularity tokamak plasmas *Rev. Mod. Plasma Phys.* **5** 6
[23] Greenwald M. *et al* 2018 The high-field path to practical fusion energy *PSFC Report PSFC/RR-18-2* (Massachusetts Institute of Technology)
[24] Hartwig Z.S. *et al* 2020 VIPER: an industrially scalable high-current high-temperature superconductor cable *Supercond. Sci. Technol.* **33** 11LT01
[25] Sheffield J. and Milora S.L. 2016 Generic magnetic fusion reactor revisited *Fusion Sci. Technol.* **70** 14–35
[26] Kikuchi M. *et al* 2014 Negative triangularity tokamak as fusion energy system *1st Int. e-Conf. on Energies* (Sciforum.net March 2014) e002
[27] Camenen Y. *et al* 2007 Impact of plasma triangularity and collisionality on electron heat transport in TCV L-mode plasmas *Nucl. Fusion* **47** 510–6
[28] Marinoni A., Brunner S., Camenen Y., Coda S., Graves J.P., Lapillonne X., Pochelon A., Sauter O. and Villard L. 2009 The effect of plasma triangularity on turbulent transport: modeling TCV experiments by linear and non-linear gyrokinetic simulations *Plasma Phys. Control. Fusion* **51** 055016
[29] Rewoldt G., Tang W.M. and Chance M.S. 1982 Electromagnetic kinetic toroidal eigenmodes for general magnetohydrodynamic equilibria *Phys. Fluids* **25** 480–90
[30] Medvedev S.Y. 2008 Beta limits and edge stability for negative triangularity plasma in TCV tokamak *35th EPS Conf. Plasma Phys.* (Hersonissos, Greece 32D (9–13 June 2008)) (http://epsppd.epfl.ch/Hersonissos/pdf2/P1_072.pdf)
[31] Medvedev S.Y. *et al* 2016 Single null divertor in negative triangularity tokamak *26th IAEA Fusion Energy Conference* (Kyoto) (17–22 Oct 2016) ICC/P3–47 (https://conferences.iaea.org/indico/event/98/session/21/contribution/3.pdf)

[32] Scott S.D., Kramer G.J., Tolman E.A., Snicker A., Varje J., Särkimäki K., Wright J.C. and Rodriguez-Fernandez P. 2020 Fast-ion physics in SPARC *J. Plasma Phys.* **86** 865860508
[33] Reux C. *et al* 2015 DEMO reactor design using the new modular system code SYCOMORE *Nucl. Fusion* **55** 073011
[34] Gray J.S., Hwang J.T., Martins J.R.R.A., Moore K.T. and Naylor B.A. 2019 OpenMDAO: an open-source framework for multidisciplinary design, analysis, and optimization *Struct. Multidiscp. Optim.* **59** 1075–104
[35] Troyon F., Gruber R., Saurenmann H., Semenzato S. and Succi S. 1984 MHD-limits to plasma confinement *Plasma Phys. Control. Fusion* **26** 209–15
[36] Sauter O. 2016 Geometric formulas for system codes including the effect of negative triangularity *Fusion Eng. Des.* **112** 633–45
[37] Troyon F. and Gruber R. 1985 A semi-empirical scaling law for the β-limit in tokamaks *Phys. Lett.* A **110** 29–34
[38] Goldston R.J. 2012 Heuristic drift-based model of the power scrape-off width in low-gas-puff H-mode tokamaks *Nucl. Fusion* **52** 013009
[39] Stangeby P.C. 2000 *The Plasma Boundary of Magnetic Fusion Devices* (*Series in Plasma Physics and Fluid Dynamics*) (London: Taylor and Francis)
[40] Anand H., Humphreys D., Eldon D., Leonard A., Hyatt A., Sammuli B. and Welander A. 2020 Plasma flux expansion control on the DIII-D tokamak *Plasma Phys. Control. Fusion* **63** 015006
[41] Loving A. *et al* 2014 Pre-conceptual design assessment of DEMO remote maintenance *Fusion Eng. Des.* **89** 2246–50
[42] Kotschenreuther M., Valanju P., Mahajan S., Zheng L.J., Pearlstein L.D., Bulmer R.H., Canik J. and Maingi R. 2010 The super X divertor (SXD) and a compact fusion neutron source (CFNS) *Nucl. Fusion* **50** 035003
[43] Goldston R.J., Myers R. and Schwartz J. 2016 The lithium vapor box divertor *Phys. Scr.* **T167** 014017
[44] Glasser A.H. 2016 The direct criterion of Newcomb for the ideal MHD stability of an axisymmetric toroidal plasma *Phys. Plasmas* **23** 072505
[45] Kesner J., Ramos J.J. and Gang F.-Y. 1995 Comet cross-section tokamaks *J. Fusion Energy* **14** 361–71
[46] D'Ippolito D.A., Freidberg J.P., Goedbloed J.P. and Rem J. 1978 High-beta tokamaks surrounded by force-free fields *Phys. Fluids* **21** 1600
[47] Wilson H.R. 1992 Bootstrap current scaling in tokamaks *Nucl. Fusion* **32** 257–63
[48] Hirshman S.P. 1988 Finite-aspect-ratio effects on the bootstrap current in tokamaks *Phys. Fluids* **31** 3150
[49] Buttery R.J. *et al* 2021 The advanced tokamak path to a compact net electric fusion pilot plant *Nucl. Fusion* **61** 046028
[50] Johner J. 2011 HELIOS: a zero-dimensional tool for next step and reactor studies *Fusion Sci. Technol.* **59** 308–49
[51] Sheffield J., Dory R.A., Cohn S.M., Delene J.G., Parsly L., Ashby D.E.T.F. and Reiersen W.T. 1986 Cost assessment of a generic magnetic fusion reactor *Fusion Technol.* **9** 199–249
[52] Ren J., Liu Y., Liu Y. and Medvedev S.Y. 2018 Feedback stabilization of ideal kink and resistive wall modes in tokamak plasmas with negative triangularity *Nucl. Fusion* **58** 126017
[53] File J., Mills R.G. and Sheffield G.V. 1971 Large superconducting magnet designs for fusion reactors *IEEE Trans. Nucl. Sci.* **18** 277–82
[54] Kikuchi M., Medvedev S., Takizuka T., Fasoli A., Wu Y., Diamond P. and Duan X. 2015 Perspective of Negative Triangularity Tokamak as Fusion Energy System *42nd European Physical Society Conf. on Plasma Physics* (Lisbon, Portugal 2015) 39E P4.179 (http://ocs.ciemat.es/EPS2015PAP/pdf/P4.179.pdf)
[55] Kramer G.J., Budny R.V., Bortolon A., Fredrickson E.D., Fu G.Y., Heidbrink W.W., Nazikian R., Valeo E. and Van Zeeland M.A. 2013 A description of the full-particle-orbit-following SPIRAL code for simulating fast-ion experiments in tokamaks *Plasma Phys. Control. Fusion* **55** 025013
[56] Kramer G.J. 2021 personal communication
[57] Kovari M., Kemp R., Lux H., Knight P., Morris J. and Ward D.J. 2014 'PROCESS': a systems code for fusion power plants: I. Physics *Fusion Eng. Des.* **89** 3054–69
[58] Wenninger R. *et al* 2017 The physics and technology basis entering European system code studies for DEMO *Nucl. Fusion* **57** 016011
[59] Ren J., Liu Y., Liu Y., Medvedev S.Y., Wang Z. and Xia G. 2016 A comparative study of ideal kink stability in two reactor-relevant tokamak plasma configurations with negative and positive triangularity *Plasma Phys. Control. Fusion* **58** 115009
[60] Head T., Kumar M., Nahrstaedt H., Louppe G. and Shcherbatyi I. 2020 Scikit-optimize/scikit-optimize *(version 0.8.1)* (https://zenodo.org/record/4014775)